Luminescent Cyanoruthenate(II)Diimine and Cyanoruthenium(II)Diimine Complexes

ARTICLE *in* CHEMISTRY - A EUROPEAN JOURNAL · NOVEMBER 2013

Impact Factor: 5.73 · DOI: 10.1002/chem.201302216 · Source: PubMed

DOI: 10.1002/chem.201302216

Luminescent Cyanoruthenate(II)–Diimine and Cyanoruthenium(II)–Diimine Complexes

Hua Feng,[a] Feng Zhang,[a, b] Sze-Wing Lai,[a] Shek-Man Yiu,[a] and Chi-Chiu Ko*[a, b]

Abstract: To improve the emission and excited-state properties of luminescent cyanometalates, new classes of highly solvatochromic luminescent cyanoruthenium(II) and cyanoruthenate(II) complexes of the general formulae $[Ru(PR_3)_2(CN)_2(\widehat{NN})]$ and $K[Ru(PR_3)(CN)_3(\widehat{NN})]$, respectively, were developed. These complexes could be readily synthesized through the ligand-substitution reaction of $K_2[Ru(CN)_4(PR_3)_2]$ with a diimine ligand. The geometrical isomerism of these complexes was characterized by using various spectroscopic techniques. Their photophysical properties, solvatochromism, and electrochemistry have also been investigated. Our detailed study showed that many of these complexes exhibited extremely environmentally sensitive emissions and significantly improved emission quantum efficiencies and lifetimes compared with the well-studied tetracyanoruthenate systems.

Keywords: coordination chemistry · electrochemistry · luminescence · ruthenium · solvatochromism

Introduction

Cyanide ligands are isoelectronic with carbonyl ligands. A comparison of their metal–ligand bonding interactions reveals that cyanide is a stronger σ-donating and weaker π-accepting ligand. Moreover, its excellent capability in bridging metal centers through a linear μ_2-C,N mode (M–C≡N–M′) is peculiar and has been well-documented.[1] Owing to the rich and unique coordination chemistry of cyanide ligands, cyanometalates have received considerable attention in various research areas, in particular in materials and supramolecular chemistry.[2]

In addition to their unique bonding features, the lone-pair of electrons on the nitrogen atoms of the cyanide ligands, which can interact with solvent molecules or electron acceptors, also gives rise to highly environmentally sensitive photophysical properties in luminescent cyanometalates.[2b,f,3] These properties have been extensively studied in the most-popular cyanoruthenate system, that is, $[Ru(CN)_4(\widehat{NN})]^{2-}$,[2f,3a–g] and they have been found to be useful in the development of luminescent chemosensors, probes, and stimuli-responsive devices.[2g,4] Although luminescent cyanometalates possess many intriguing and favorable properties, modification of their properties is challenging when the only modifiable diimine ligand is functionalized for various applications. Moreover, the luminescent quantum yields and emission lifetimes of most of these cyanometalates are very low,[2f,3] thereby limiting the performance of their applications. Replacing the metal center is one possible strategy for tuning the properties of cyanometalates and does not require the redesign of the functionalized diimine ligand.[2f,3g,h,i] In this context, we recently developed a new family of cyanorhenate–diimine complexes.[3i] Although luminescent cyanometalates with different metal centers, such as Os, Ir, and Re, have been explored, the emission quantum yields and lifetimes of many of these complexes remain unsatisfactory.[2f,3]

To improve the luminescence and excited-state properties of these complexes, we proposed replacing one or two of the cyanide ligands in the tetracyanoruthenate–diimine complexes with much-better π-accepting phosphine ligands to raise their emissive metal-to-ligand charge transfer (MLCT) state, which may impede the thermal-deactivation pathway. In addition, variation of the substituents on the phosphine ligand provides a possible means of modifying the physical and excited-state properties of these complexes.[5] Herein, we report the synthesis, structures, photophysical properties, and electrochemistry of a new series of highly luminescent phosphino–cyanoruthenate(II)–diimine and cyanoruthenium(II)–diimine complexes. Because these complexes were inevitably become less sensitive towards changes in their microenvironment compared to the tetracyanoruthenate(II)–diimine complexes, we also investigated their solvatochromism.

[a] Dr. H. Feng, F. Zhang, S.-W. Lai, Dr. S.-M. Yiu, Dr. C.-C. Ko
Department of Biology and Chemistry, City University of Hong Kong
Tat Chee Avenue, Kowloon, Hong Kong (P.R. China)
Fax: (+852) 3442-0522
E-mail: vinccko@cityu.edu.hk

[b] F. Zhang, Dr. C.-C. Ko
Advanced Laboratory for Environmental Research and Technology (ALERT)
USTC-CityU Joint Advanced Research Center
Suzhou, Jiangsu 215123 (P.R. China)

Supporting information for this article is available on the WWW under http://dx.doi.org/10.1002/chem.201302216.

Results and Discussion

Synthesis and characterization: The target phosphino–tricyanoruthenate(II)–diimine and phosphino–dicyanoruthenium(II)–diimine complexes were obtained from substitution reactions between the diphosphino–tetracyanoruthenate precursor complexes, $K_2[Ru(CN)_4(PR_3)_2]$, and the diimine ligands (Scheme 1). These precursor complexes could

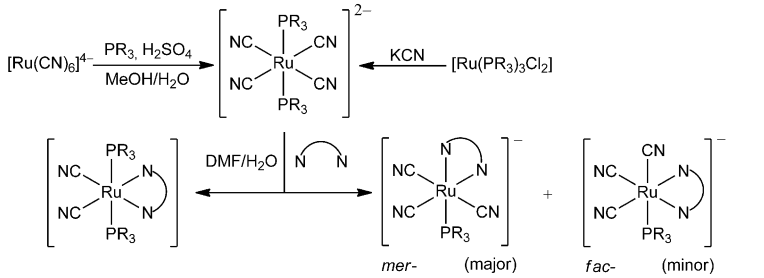

1: R = Ph; N-N = bpy
3: R = Ph; N-N = Me_2bpy
5: R = Ph; N-N = phen
7: R = tol; N-N = bpy
9: R = C_6H_4Cl; N-N = bpy
11: R = C_6H_4OMe; N-N = bpy

2: R = Ph; N-N = bpy
4a: R = Ph; N-N = Me_2bpy
6: R = Ph; N-N = phen
8: R = tol; N-N = bpy
10: R = C_6H_4Cl; N-N = bpy
12: R = C_6H_4OMe; N-N = bpy

4b: R = Ph; N-N = Me_2bpy

Scheme 1. Synthetic route to $[Ru(PR_3)_2(CN)_2(\widehat{NN})]$ and $K[Ru(PR_3)(CN)_3(\widehat{NN})]$.

be prepared by the reactions between KCN and $[Ru(PR_3)_3Cl_2]$ or by the reactions between the corresponding phosphine and $K_4[Ru(CN)_6]$. Because the ligand-substitution reaction of $[Ru(PR_3)_3Cl_2]$ required a large excess of KCN, which was difficult to remove from the reaction mixture and was extremely poisonous, we used the ligand-substitution reactions of $K_4[Ru(CN)_6]$ with 2.2 molar equivalents of the phosphine ligands at reflux in an aqueous solution of MeOH under acidic conditions to prepare the precursor complexes.

The substitution reactions between $K_2[Ru(CN)_4(PR_3)_2]$ and 1.2 molar equivalents of the corresponding diimine ligand at reflux in DMF/H_2O (2:1 v/v) produced mixtures of the target complexes, $[Ru(PR_3)_2(CN)_2(\widehat{NN})]$ and $K[Ru(PR_3)(CN)_3(\widehat{NN})]$, in ratios from 1:3 to 2:3 (Scheme 1). Owing to the charge difference between these complexes, they could be readily separated by column chromatography on alumina by using CH_2Cl_2/MeOH as the eluent. The tricyano–ruthenate complexes that were obtained from these reactions, $K[Ru(PR_3)(CN)_3(\widehat{NN})]$, mainly adopted a meridional configuration, which could be characterized by two sets of ^{1}H NMR signals for the chemically inequivalent pyridyl protons on the diimine ligand. Trace amounts of the facial isomer could also be isolated by chromatographic purification. This result was confirmed by a full characterization of the minor product (**4b**) following a large-scale reaction between $K_2[Ru(CN)_4(PPh_3)_2]$ and Me_2bpy. All of the target complexes were air and thermally stable. The neutral complexes, $[Ru(PR_3)_2(CN)_2(\widehat{NN})]$, showed good solubility in non-polar organic solvents, but they were sparingly soluble in polar organic solvents and insoluble in water, whereas the potassium salt of the anionic ruthenate complexes, $K[Ru(PR_3)(CN)_3(\widehat{NN})]$, were only soluble in polar organic solvents and water. All of the complexes gave satisfactory elemental analysis data and were characterized by ^{1}H NMR spectroscopy, IR spectroscopy, and ESI mass spectrometry. Complexes **3**, **4b**, and **11** were also structurally characterized by X-ray crystallography.

IR and NMR spectroscopy: The geometrical isomerism of the precursor and target complexes was elucidated by using NMR and IR spectroscopy. The *trans*-geometrical isomerism of the precursor complexes, $K_2[Ru(CN)_4(PR_3)_2]$, was confirmed by the observation of one IR-active C≡N stretch in the IR spectra[6] and by one ^{13}C NMR signal for all four cyanide ligands (see the Supporting Information, Figure S1). These results were consistent with the symmetrical environment around the cyanide ligands in an octahedral complex with D_{4h} symmetry. The virtual triplet for the ^{13}C NMR signals of the phosphine ligands (see the Supporting Information, Figure S1) arose from coupling between the C atom and two chemically equivalent (but magnetically inequivalent) phosphorus nuclei, which were strongly coupled through the ruthenium metal center. This result is consistent with a *trans*-phosphine arrangement and is typically observed in *trans*-phosphine–transition-metal complexes.[7] The target dicyano and tricyano complexes were characterized by two and three IR-active C≡N stretches, respectively, within the region 2050–2100 cm^{-1}. Although the *mer*- and *fac*-isomers of the tricyano ruthenate complexes, $K[Ru(PR_3)(CN)_3(\widehat{NN})]$, could not be distinguished by the number of IR-active C≡N stretches, they could be readily differentiated by the ^{1}H NMR signals of their diimine ligands. In the *mer*-isomeric form, the two pyridyl moieties of the diimine were *trans* to different ligands and, therefore, were chemically inequivalent, thus leading to two sets of ^{1}H NMR signals for each pyridyl moiety (Figure 1a). In contrast, the two pyridyl moieties of the diimine were both *trans* to cyano ligands in the *fac*-isomer and, thus, their protons only exhibited one set of ^{1}H NMR signals (Figure 1b). There are three possible geometrical isomeric forms of the dicyanoruthenium complexes, $[Ru(PR_3)_2(CN)_2(\widehat{NN})]$: 1) *cis*,*cis*; 2) *cis*-cyano,*trans*-phosphino (*cis*,*trans*); and 3) *trans*-cyano,*cis*-phosphino (*trans*,*cis*). The observations of two IR-active C≡N stretches in the IR spectra and the symmetrical environment of the two pyridyl protons of the diimine ligand in the NMR spectra excluded the *trans*,*cis* and *cis*,*cis* geometrical arrangements, respectively. The *cis*,*trans* isomerism of these

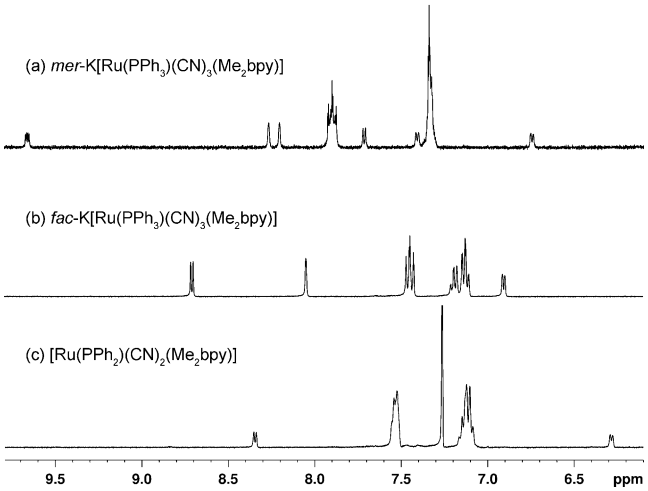

Figure 1. ^{1}H NMR spectra of a) compound **4a**, b) compound **4b**, and c) compound **3**.

complexes was further confirmed from the X-ray crystal structures of compounds **3** and **11**.

X-ray crystal-structure determination: Single crystals of complexes **3**, **4b**, and **11** suitable for X-ray diffraction were obtained by the slow diffusion of Et_2O vapor into concentrated solutions of the complexes CH_2Cl_2/MeOH (10:1 v/v). ORTEPs of these complexes are shown in Figure 2. The experimental details for the crystal-structure determinations and the selected bond lengths and angles are summarized in the Supporting Information, Table S1 and Table 1, respectively. The ruthenium metal centers of these structures adopted a distorted octahedral geometry and the geometrical arrangement of the ligands was consistent with the proposed isomerism based on the IR and NMR spectroscopic data. As with other bipyridyl–transition-metal complexes,[2c,3d,h,8] the N-Ru-N angles were typically within the range 77.0–78.4°. The Ru–CN and C≡N bond lengths were within the ranges 2.00–2.05 Å and 1.15–1.17 Å, respectively, which were comparable with those in $[Ru(\widehat{NN})(CN)_4]^{2-}$[2c,3c,4a] and the free CN^- anion (1.16 Å).[9] In tricyanoruthenate complex **4b**, the Ru–CN bond length for the cyanide ligand (2.05 Å) *trans* to the phosphine ligand was slightly longer than those (2.00 Å) *trans* to the diimine ligand. This difference was probably due to the stronger *trans* influence and π-accepting ability of the phosphine ligands compared with the diimine ligands. The Ru–N (2.09–2.12 Å) and Ru–P (2.34–2.37 Å) bond lengths in these complexes were also within the typical ranges of other ruthenium(II)–bipyridine[2c,3d] and ruthenium(II)–phosphine complexes.[10]

UV/Vis absorption and emission properties: Because all of these complexes showed good solubility in EtOH, their electronic absorption and emission properties in EtOH (Table 2) were compared and are discussed as follows. All of these complexes exhibited intense absorptions within the range 230–320 nm, which corresponded to the ligand-centered (LC) π–π* absorptions of the phosphine and bipyridine ligands. This assignment was further supported by the generally higher absorptivities of the $[Ru(PR_3)_2(CN)_2(\widehat{NN})]$ complexes compared to the $K[Ru(PR_3)(CN)_3(\widehat{NN})]$ complexes, because the dicyano complexes contained one more phosphine ligand. In the near-UV/Vis region, all of the complexes showed a moderately intense absorption, with molar absorptivities in the order of $10^3\,M^{-1}cm^{-1}$. With reference to

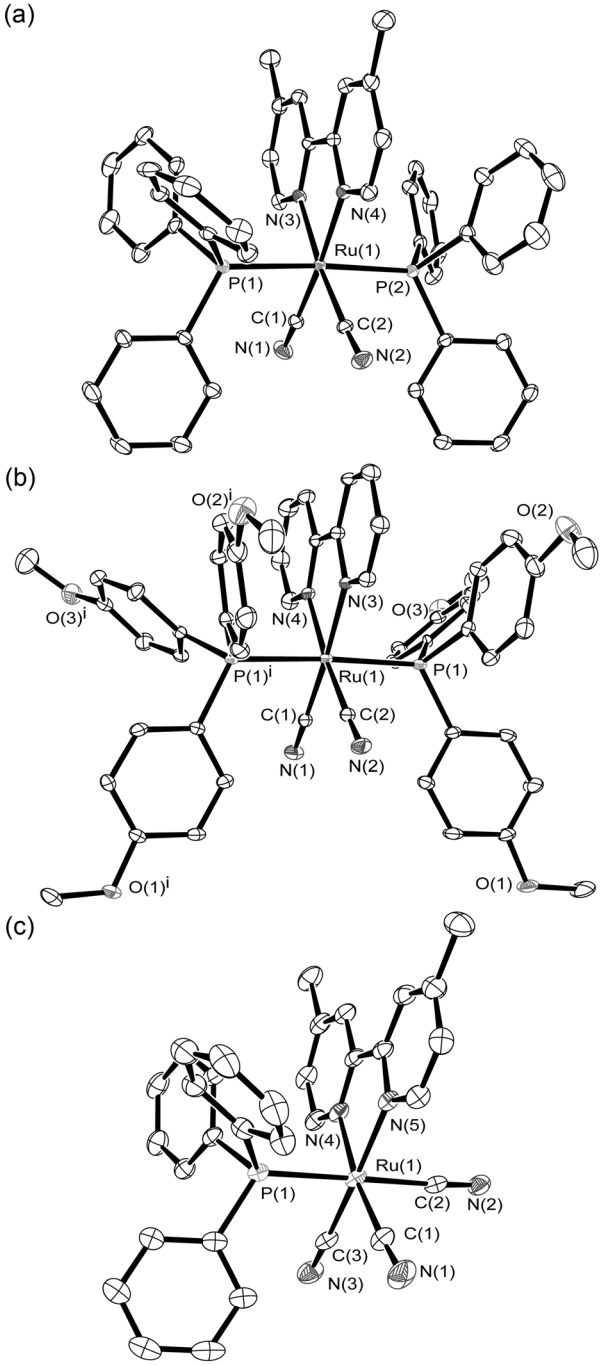

Figure 2. ORTEP drawings of a) compound **3**, b) compound **11**, and c) the anion of complex **4b**. Thermal ellipsoids are set at 30% probability; hydrogen atoms are omitted for clarity.

Table 1. Selected bond lengths [Å] and angles [°] in the crystal structures of **3**, **4b**, and **11**; estimated standard deviations are given in parentheses.

3			
Ru(1)–C(1)	1.994(3)	Ru(1)–C(2)	2.005(3)
Ru(1)–N(3)	2.109(2)	Ru(1)–N(4)	2.125(3)
Ru(1)–P(2)	2.3567(7)	Ru(1)–P(1)	2.3653(7)
C(1)–N(1)	1.156(5)	C(2)–N(2)	1.152(5)
N(3)-Ru(1)-N(4)	77.13(10)	C(1)-Ru(1)-C(2)	94.75(13)
C(2)-Ru(1)-N(4)	94.69(12)	C(1)-Ru(1)-N(3)	93.42(11)
4b			
Ru(1)–C(1)	2.005(4)	Ru(1)–C(2)	2.049(4)
Ru(1)–C(3)	2.003(4)	Ru(1)–N(4)	2.116(3)
Ru(1)–N(5)	2.123(3)	Ru(1)–P(1)	2.3418(10)
C(1)–N(1)	1.154(6)	C(2)–N(2)	1.150(5)
C(3)–N(3)	1.153(6)		
N(4)-Ru(1)-N(5)	77.11(12)	C(1)-Ru(1)-C(2)	96.21(18)
C(1)-Ru(1)-N(4)	172.38(16)	C(2)-Ru(1)-N(5)	86.88(13)
C(1)-Ru(1)-C(2)	96.21(18)	C(2)-Ru(1)-C(3)	90.09(16)
11			
Ru(1)–C(1)	2.030(8)	Ru(1)–C(2)	2.018(8)
Ru(1)–N(3)	2.127(6)	Ru(1)–N(4)	2.130(6)
Ru(1)–P(2)	2.3465(12)	Ru(1)–P(1)	2.3465(12)
C(1)–N(1)	1.135(11)	C(2)–N(2)	1.153(10)
N(3)-Ru(1)-N(4)	77.4(3)	C(1)-Ru(1)-C(2)	93.5(3)
C(1)-Ru(1)-N(3)	172.5(3)	C(2)-Ru(1)-N(4)	171.3(3)

previous spectroscopic studies on $[Ru(bpy)(CN)_4]^{2-}$,[3a,b,4b] this absorption was similarly assigned to $[d\pi(Ru)\rightarrow\pi^*(\widehat{NN})]$ MLCT transitions. Their absorption maxima showed a dependence on the electron nature of the ligands: 1) in line with the π-accepting ability of the diimine ligand (bpy > Me_2bpy) for complexes with the same ancillary ligands (**1** (412 nm) > **3** (408 nm); **2** (419 nm) > **4a** (411 nm)) and 2) in accordance with the decreasing π-accepting ability of all of the other ancillary ligands; thus, the absorption maxima followed the trend tricyanoruthenate(II) complexes > dicyanoruthenium(II) complexes, that is, $K[Ru(PR_3)(CN)_3(\widehat{NN})] > [Ru(PR_3)_2(CN)_2(\widehat{NN})]$, with identical phosphine and diimine ligands. The maxima also decreased with decreasing π-accepting ability of the phosphine ligands, $P(C_6H_4OMe)_3 < P(tol)_3 < PPh_3 < P(C_6H_4Cl)_3$, for each series of complexes with the same diimine ligand (**11** (421 nm) > **7** (418 nm) > **1** (412 nm) > **9** (402 nm) and **12** (426 nm) > **8** (423 nm) > **2** (419 nm) > **10** (412 nm)). These trends were in agreement with the influence of the ligands on the energy of the orbitals that were involved in the MLCT transition $[d\pi(Ru)\rightarrow\pi^*(\widehat{NN})]$.

Similar to tetracyanoruthenate–diimine complexes,[2b,f,3a,4b] these complexes (**1**–**12**) also displayed strong solvatochromism, owing to their solvent-sensitive MLCT transitions, with a significant blue-shift on moving from non-polar solvents to polar and protic solvents (Figure 3 and the Supporting Information, Table S2). Such solvatochromic behavior was similarly ascribed to the interaction between the solvent and the electron lone-pair of the nitrogen atoms of the cyanide ligands. Consequently, the degree of solvatochromic behavior of the MLCT transitions was in line with the number of cya-

Table 2. Photophysical data for complexes **1**–**12**.

	Medium (T [K])	Emission[a] λ_{em} [nm] (τ_o [μs])	ϕ_{em}[b] ($\times 10^3$)	Absorption[c] λ_{abs} [nm] (ε [$dm^3mol^{-1}cm^{-1}$])
1	EtOH (298)	561 (0.040)	7.1	226 sh (49710), 276 (16160), 253 (37365), 310 sh (10975), 412 (3305)
	glass[d] (77)	502 (11.7)		
2	EtOH (298)	608 (0.475)	28.7	222 sh (37300), 291 (23155), 317 sh (5935), 419 (3975)
	glass[d] (77)	537 (6.95)		
3	EtOH (298)	553(0.011)	5.0	222 sh (52790), 254 (36920), 291 (20155), 308 sh (10390), 408 (3160)
	glass[d] (77)	500 (11.9)		
4a	EtOH (298)	600 (0.372)	47.3	220 sh (24580), 250 sh (7300), 288 (12790), 307 (4320), 411 (2120)
	glass[d] (77)	535 (6.38)		
4b	EtOH (298)	597 (0.698)	89.1	220 sh (40790), 250 sh (11760), 288 (20745), 310 sh (6315), 413 (3465)
	glass[d] (77)	523 (8.34)		
5	EtOH (298)	547 (0.082)	8.3	220 sh (67614), 256 (45555), 284 sh (14515), 316 sh (6165), 387 (4645)
	glass[d] (77)	505 (40.6)		
6	EtOH (298)	600 (2.745)	100.7	225 (52250), 266 (36505), 285 sh (11865), 316 sh (2955), 407 (5240)
	glass[d] (77)	542 (17.7)		
7	EtOH (298)	565 (0.088)	10.3	234 (57935), 258 sh (41555), 294 (19300), 309 sh (11615), 418 (2980)
	glass[d] (77)	508 (12.7)		
8	EtOH (298)	611 (0.439)	20.3	224 sh (34780), 254 sh (12030), 291 (19510), 322 sh (4980), 423 (3455)
	glass[d] (77)	536 (6.23)		
9	EtOH (298)	611 (0.609)	8.7	237 (65600), 258 sh (45115), 290 (18930), 310 (10185), 402 (2825)
	glass[d] (77)	492 (11.2)		
10	EtOH (298)	596 (0.522)	34.1	236 (39730), 289 (20440), 310 (6760), 412 (3460)
	glass[d] (77)	536 (7.41)		
11	EtOH (298)	570 (0.241)	25.0	245 (72795), 263 sh (52195), 290 (20930), 308 sh (12070), 421 (2675)
	glass[d] (77)	518 (14.3)		
12	EtOH (298)	613 (0.522)	25.3	241 (46040), 290 (23455), 312 sh (6455), 426 (3860)
	glass[d] (77)	544 (6.13)		

[a] Excitation at 400 nm. [b] Luminescence quantum yield on excitation at 436 nm. [c] in EtOH at 298 K. [d] In EtOH/MeOH (4:1, v/v).

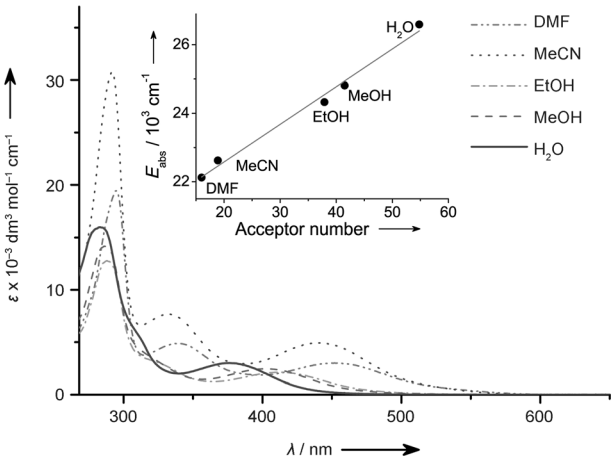

Figure 3. UV/Vis absorption spectra of compound **4a** in various solvents. Inset shows a plot of the absorption energy (E_{abs}) of the lowest-energy MLCT absorption band of compound **4a** versus the acceptor number of the solvent.

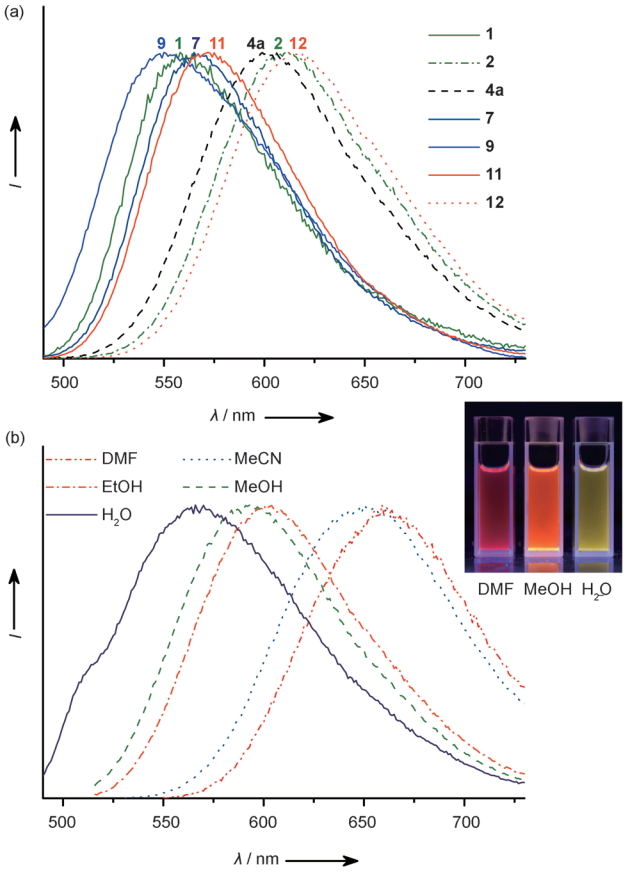

Figure 4. Emission spectra of a) selected complexes in EtOH at 298 K and b) compound **4a** in various solvents.

nide ligands in the complexes[3b] and, thus, the shifts in their lowest-energy MLCT bands on switching from DMF to MeOH followed the order: $[Ru(CN)_4(bpy)]^{2-}$ (4330 cm^{-1})[3b] > $[Ru(CN)_3(PR_3)(bpy)]^-$ (2600–2900 cm^{-1}) > $[Ru(CN)_2(PR_3)_2(bpy)]$ (750–1200 cm^{-1}). Analogous to the tetracyanoruthenate complexes,[3b] the MLCT absorption energy of the tricyanoruthenate complexes, $[Ru(CN)_3(PR_3)(\widehat{NN})]^-$, in different solvents showed a linear correlation with the acceptor number of the solvent (Figure 3). In contrast, the MLCT absorption of the diphosphino–dicyanoruthenium complexes, $[Ru(CN)_2(PR_3)_2(\widehat{NN})]$, did not show a good correlation with the acceptor number of the solvent (see the Supporting Information, Figure S2), but instead showed a linear correlation with Dimroth's solvent parameter.[11] This result indicated that the solvatochromism of these dicyano complexes arose more than from the interaction between the solvent and the lone pair electrons of the cyanide ligands as the number of cyanide ligands decreased.[3b]

All of the complexes displayed greenish yellow to red MLCT phosphorescence in degassed EtOH solution at 298 K (Figure 4, Table 2) with sub-microsecond emission lifetimes and quantum yields (ϕ_{436}) of up to 10.1 %; these values were significantly enhanced compared with that of the tetracyanoruthenate(II)–bipyridyl complex, $[Ru(CN)_4(bpy)]^{2-}$ (0.7 % in H_2O[3a,f] and 0.2 % in MeOH[3f]). The much-higher luminescence quantum efficiencies of these complexes compared with those of the tetracyanoruthenate complexes was due to the raised energy of the ^{3}MLCT emissive state, which impeded the thermal-deactivation pathway, through the replacement of one or two of the cyano ligands with better π-accepting phosphine ligands. On the other hand, because the ligand-field strength of the cyanide ligand is mainly derived from its strong σ-donation,[12] replacing one of the cyanide ligands with the strongly σ-donating and much-better π-accepting phosphine ligands may also raise the deactivating ligand-field excited state. The emission energy was in line with the π-accepting ability of the ancillary ligands for the same complex system and followed the order: $[Ru(CN)_2(PR_3)_2(\widehat{NN})] > [Ru(CN)_3(PR_3)(\widehat{NN})]^- > [Ru(CN)_4(\widehat{NN})]^{2-}$. These trends were in agreement with the assignment of the ^{3}MLCT excited state. The MLCT phosphorescence properties of these complexes also exhibited a strong dependence on the solvent (Figure 4b and the Supporting Information, Table S2), with similar trends to the MLCT absorptions. Although the emission properties of $[Ru(CN)_3(PR_3)(\widehat{NN})]^-$ were less sensitive to the microenvironment than those of $[Ru(CN)_4(bpy)]^{2-}$, their emission colors in different solvents were readily distinguishable to the naked eyes (Figure 4b). The environmentally sensitive emission of these complexes could cover a broader color range in the visible-light region, from green to red, by slightly raising the energy of the MLCT emissive states. This result could be simply and readily achieved through a slight modification of the π-accepting ability of the phosphine and diimine ligands of the complexes. In EtOH/MeOH glassy medium at 77 K, these complexes displayed stronger and blue-shifted MLCT phosphorescence (Table 2 and the Supporting Information, Figure S3), with similar trends in the emission energy to those in the solution state. This result was due to the rigidochromic effect and such an effect is commonly observed in MLCT emitters.[11c,d,13]

Electrochemistry: The electrochemical properties of all of these complexes in MeCN with 0.1 M nBu$_4$NPF$_6$ were investigated by using cyclic voltammetry. All of the complexes showed a quasi-reversible metal-centered ($Ru^{III/II}$) oxidative couple within the range +0.67 to +1.09 V vs. SCE (Figure 5, Table 3). The metal-centered oxidation assignment was supported by the lower oxidative potentials for the more-electron-rich tricyanoruthenate complexes, $[Ru(CN)_3(PR_3)(\widehat{NN})]^-$ (+0.67 to +0.79 V), than for the dicyanoruthenium complexes, $[Ru(CN)_2(PR_3)_2(\widehat{NN})]$ (+0.93 to +1.09 V). This result was further supported by the trends of the potentials of each series of complexes, which were in line with the π-accepting ability of the phosphine ligands in the bipyridyl complexes. These oxidation potentials were much more anodic than that of $[Ru(CN)_4(bpy)]^{2-}$ (+0.27 V vs. SCE in MeCN),[2b,14] thus suggesting that the dπ orbitals of the Ru^{II} metal center were significantly stabilized on replacement of the cyanide ligand with the phosphine ligand. As a result, the MLCT transition and the phosphorescence of these complexes were also considerably blue-shifted compared with those of $[Ru(CN)_4(bpy)]^{2-}$. In water, the metal-centered oxidations of the cyanoruthenates (**2**, **4**, **6**, **8**, **10**, and **12**) were irreversible and within the range +0.94 to +1.06 V (see the Supporting Information, Table S3). In the reductive scan, a quasi-reversible diimine-based reduction couple within the range −1.74 to −1.93 V vs. SCE was observed for all of the complexes.

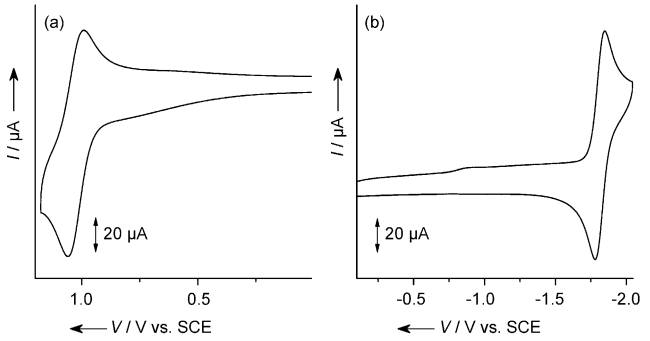

Figure 5. Cyclic voltammograms of the a) oxidative and b) reductive scans of compound **3** in MeCN with 0.1 mol dm^{-3} nBu$_4$NPF$_6$.

Table 3. Electrochemical data for complexes **1**–**12** in MeCN with 0.1 mol dm^{-3} nBu$_4$NPF$_6$ at 298 K.[a]

Complex	Oxidation $E_{1/2}$ (vs. SCE) [V][b] (ΔE_p [mV])[c]	Reduction $E_{1/2}$ (vs. SCE) [V][b] (ΔE_p [mV])[c]
1	–[d]	–[d]
2	+0.70 (67)	−1.81 (69)
3	+1.03 (77)	−1.81 (70)
4a	+0.69 (77)	−1.92 (70)
4b	+0.68 (68)	−1.93 (70)
5	+1.09 (80)	−1.74 (67)
6	+0.71 (69)	−1.80 (70)
7	–[d]	–[d]
8	+0.67 (69)	−1.82 (77)
9	–[d]	–[d]
10	+0.79 (65)	−1.77 (69)
11	+0.93 (74)	−1.75 (81)
12	+0.67 (85)	−1.83 (81)

[a] Working electrode: glassy carbon, scan rate: 100 mV s^{-1}. [b] $E_{1/2} = (E_{pa}+E_{pc})/2$, where E_{pa} and E_{pc} are the anodic and cathodic peak potentials, respectively. [c] $\Delta E_p = |E_{pa}-E_{pc}|$. [d] Owing to the limited solubility of the complexes, the data cannot be determined with accuracy.

Conclusion

New classes of highly solvatochromic luminescent cyanoruthenium(II) and cyanoruthenate(II) complexes have been developed. These complexes showed extremely environmentally sensitive emissions and significantly improved emission quantum efficiencies and lifetimes compared with the well-studied tetracyanoruthenate systems. Given their photophysical properties, these complexes hold great promise for applications as luminescent materials, photosensitizers, and as building blocks for the development of luminescent probes and sensors. Moreover, the presence of potentially bridging cyanide ligands in these complexes also allows for the development of coordination polymers and networks.

Experimental Section

Materials and reagents: Diimine ligands, 1,10-phenanthroline (phen), 2,2′-bipyridine (bpy), and 4,4′-dimethyl-2,2′-bipyridine (Me_2bpy) were purchased from Acros Organics. The phosphine ligands, triphenylphosphine, tri-*p*-tolylphosphine [P(tol)$_3$], tris(*p*-chlorophenyl)phosphine [P(C$_6$H$_4$Cl)$_3$], and tris(*p*-methoxyphenyl)phosphine [P(C$_6$H$_4$OMe)$_3$], and $RuCl_3$ were purchased from Strem Chemical Company. These commercially available reagents were used without further purification. [Ru(PR$_3$)$_3$Cl$_2$][15] and K$_4$[Ru(CN)$_6$][16] were synthesized according to literature procedures. All of the other reagents and solvents were of analytical grade and were used without further purification.

Physical measurements and instrumentation: ^{1}H NMR spectra were recorded on a Bruker AV400 (400 MHz) FT-NMR spectrometer. Chemical shifts (δ) are reported relative to tetramethylsilane (Me_4Si). All negative/positive-ion ESI mass spectra were recorded on a PE-SCIEX API 150 EX single-quadruple mass spectrometer. Elemental analysis was performed on an Elementar Vario MICRO Cube elemental analyzer. IR spectra of the solid samples as KBr discs were obtained within the range 4000–400 cm^{-1} on an AVATAR 360 FTIR spectrometer.

All of the electronic absorption spectra were recorded on a Hewlett–Packard 8453 or Hewlett–Packard 8452A diode-array spectrophotometer. Steady-state emission and excitation spectra were measured at RT and at 77 K on a Horiba Jobin Yvon Fluorolog-3-TCSPC spectrofluorometer. The solutions were rigorously degassed on a high-vacuum line in a two-compartment cell with not less than four successive freeze–pump–thaw cycles. The measurements at 77 K were carried out on dilute solutions of the samples in EtOH/MeOH (4:1 v/v) loaded in a quartz tube inside a quartz-walled Dewar flask that contained liquid nitrogen. The luminescence quantum yields were determined by using the optical-dilution method as described by Demas and Crosby[17] with an aerated aqueous solution of [Ru(bpy)$_3$Cl$_2$] ($\phi_{em} = 0.040$[18] with excitation at 436 nm) as the reference. Luminescence lifetimes were measured by using the time-correlated single-photon-counting (TCSPC) technique on a Fluorolog-3-TCSPC spectrofluorometer in a fast MCS mode with a NanoLED-375 LH excitation source, which had a peak excitation wavelength at 375 nm and a pulse width of less than 750 ps. The photon-counting data were analyzed on Horiba Jobin Yvon Decay Analysis Software.

Cyclic voltammetric measurements were performed on a CH Instruments, Inc. Model CHI 620 Electrochemical Analyzer. Electrochemical measurements were performed in MeCN solution with nBu$_4$NPF$_6$ (0.1 M) as a supporting electrolyte at RT. The reference electrode was a Ag/AgCl (0.1 M in MeCN) electrode and the working electrode was a glassy carbon electrode (CH Instruments, Inc.) with platinum wire as the counter electrode. The surface of the working electrode was polished with a 1 μm α-alumina slurry (Linde) and then with a 0.3 μm α-alumina slurry (Linde) on a microcloth (Buehler Co.). The ferrocenium/ferrocene couple ($FeCp_2^{+/0}$) was used as an internal reference. All of the solutions for the electrochemical studies were de-aerated with pre-purified argon gas prior to the measurements.

X-ray crystal-structure determination: The crystal structures were determined on an Oxford Diffraction Gemini S Ultra X-ray single-crystal diffractometer by using graphite-monochromated $Cu_{K\alpha}$ radiation (λ = 1.5417). The structures were solved by using direct methods with the SHELXS-97 program.[19] The Ru atoms and many of the non-hydrogen atoms were located according to the direct methods. The positions of the other non-hydrogen atoms were located after refinement by full-matrix least-squares by using the SHELXL-97 program.[19] In the final stage of the least-squares refinement, all non-hydrogen atoms were refined anisotropically. H atoms were generated by using the SHELXL-97 program.[19] The positions of H atoms were calculated based on the riding model with thermal parameters that were 1.2 times that of the associated C atoms and participated in the calculation of the final R indices.

CCDC-943828 (**3**), CCDC-943830 (**4b**), and CCDC-943829 (**11**) contain the supplementary crystallographic data for this paper. These data can be obtained free of charge from The Cambridge Crystallographic Data Centre via www.ccdc.cam.ac.uk/data_request/cif.

Syntheses: All of the reactions were carried out under strictly anaerobic conditions in an inert argon atmosphere by using standard Schlenk techniques.

General procedure for the synthesis of $K_2[Ru(PR_3)_2(CN)_4]$ (PR_3 = PPh_3, $P(tol)_3$, $P(C_6H_4Cl)_3$, $P(C_6H_4OMe)_3$): The precursor complexes, potassium tetracyanodiphosphino ruthenate(II)s, were synthesized through a ligand-substitution reaction between potassium hexacyanoruthenate(II) and the phosphine ligands under acidic conditions. To a solution of $K_4[Ru(CN)_6]$ (0.5 g) in MeOH/H_2O (25 mL, 1:1 v/v) was added the phosphine ligand (2.2 mol. equiv). The pH value of the mixture was adjusted to pH 3–4 by the addition of concentrated sulfuric acid. Then, the resulting mixture was heated at reflux for 10 h. After cooling to RT, the solution was neutralized with an aqueous solution of $KHCO_3$ (2 M) and dried by rotary evaporation. The residue was washed with copious amounts of Et_2O to remove excess phosphine ligand to obtain the crude product. Further purification of the precursor complexes could be performed by filtering through a short column of alumina (MeOH/MeCN, 1:1 v/v) and recrystallization from hot MeOH.

General procedure for the synthesis of $[Ru(PR_3)_2(CN)_2(\widehat{NN})]$ and $K[Ru(PR_3)(CN)_3(\widehat{NN})]$ (Scheme 1**)**: A mixture of $K_2[Ru(PR_3)_2(CN)_4]$ (0.25 g) and the corresponding diimine ligand (1.2 equiv) in DMF/H_2O (15 mL, 2:1 v/v) was heated at reflux overnight. After removal of the solvent under reduced pressure, the residue was washed with Et_2O and purified by column chromatography on alumina (CH_2Cl_2/MeOH) to give $[Ru(PR_3)_2(CN)_2(\widehat{NN})]$ (first band) and *mer*-$K[Ru(PR_3)(CN)_3(\widehat{NN})]$ (second band). Analytically pure yellow crystalline solids of $[Ru(CN)_2(PR_3)_2(\widehat{NN})]$ and orange/red crystalline solids of $K[Ru(CN)_3(PR_3)(\widehat{NN})]$ were obtained by recrystallization (slow diffusion of Et_2O vapor into concentrated solutions of these complexes in CH_2Cl_2/MeOH).

$[Ru(PPh_3)_2(CN)_2(bpy)]$ (1): Yield: 14.3 % (37 mg, 0.044 mmol); ^{1}H NMR (400 MHz, $CDCl_3$): δ = 8.54 (d, J = 4.9 Hz, 2H; 6,6′-bpy H), 7.71 (d, J = 8.2 Hz, 2H; 3,3′-bpy H), 7.56–7.48 (m, 12H; phenyl H), 7.42 (t, J = 7.6 Hz, 2H; 5,5′-bpy H), 7.19–7.07 (m, 18H; phenyl H), 6.48 ppm (t, J = 6.5 Hz, 1H; 4,4′-bpy H); ^{31}P NMR (162 MHz, $CDCl_3$): δ = 37.82 ppm; IR (KBr disc): $\tilde{\nu}$ = 2077, 2060 cm^{-1} (C≡N); MS (ESI, positive-ion mode): m/z 856.6 $[M+Na]^+$; elemental analyses calcd (%) for **1**·0.5H_2O: C 68.40, H 4.66, N 6.65; found: C 68.11, H 4.96, N 6.67.

***mer*-K[Ru(PPh$_3$)(CN)$_3$(bpy)] (2)**: Yield: 27.5 % (54 mg, 0.085 mmol); ^{1}H NMR (400 MHz, MeOD): δ = 9.87 (m, 1H; 6-bpy H), 8.42 (d, J = 7.6 Hz, 1H; 3-bpy H), 8.36 (d, J = 8.1 Hz, 1H; 3′-bpy H), 8.04 (td, J = 8.0, 1.5 Hz, 1H; 4-bpy H), 7.96–7.88 (m, 7H; phenyl H, 6′-bpy H), 7.86 (td, J = 8.0, 1.5 Hz, 1H; 4′-bpy H), 7.59 (t, J = 6.6 Hz, 1H; 5-bpy H), 7.40–7.29 (m, 9H; phenyl H), 6.92 ppm (ddd, J = 7.1, 5.6, 1.2 Hz, 1H; 5′-bpy H); ^{31}P NMR (162 MHz, MeOD): δ = 58.79 ppm; IR (KBr disc): $\tilde{\nu}$ = 2096, 2067, 2054 cm^{-1} (C≡N); MS (ESI, negative-ion mode): m/z 598.2 $[M-K]^-$; elemental analyses calcd (%) for **1**·2H_2O: C 55.35, H 4.05, N 10.41; found: C 55.38, H 4.17, N 10.22.

$[Ru(PPh_3)_2(CN)_2(Me_2bpy)]$ (3): Yield: 15.8 % (42 mg, 0.049 mmol); ^{1}H NMR (400 MHz, $CDCl_3$): δ = 8.34 (d, J = 5.7 Hz, 2H; 6,6′-bpy H), 7.56–7.50 (m, 14H; phenyl and 3,3′-bpy H), 7.17–7.08 (m, 18H; phenyl H), 6.28 (d, J = 5.8 Hz, 2H; 5,5′-bpy H), 2.29 ppm (s, 6H; methyl H); ^{31}P NMR (162 MHz, $CDCl_3$): δ = 37.88 ppm; IR (KBr disc): $\tilde{\nu}$ = 2077, 2062 cm^{-1} (C≡N); MS (ESI, positive-ion mode): m/z 863.1 $[M+H]^+$; elemental analyses calcd (%) for **3**·H_2O: C 68.25, H 5.04, N 6.37; found: C 68.36, H 4.65, N 6.17.

***mer*-K[Ru(PPh$_3$)(CN)$_3$(Me$_2$bpy)] (4a)**: Yield: 27.2 % (56 mg, 0.084 mmol); ^{1}H NMR (400 MHz, MeOD): δ = 9.67 (m, 1H; 6-bpy H), 8.27 (s, 1H; 3-bpy H), 8.21 (s, 1H; 3′-bpy H), 7.94–7.86 (m, 6H; phenyl H), 7.72 (d, J = 5.8 Hz, 1H; 6′-bpy H), 7.41 (d, J = 5.7 Hz, 1H; 5-bpy H), 7.39–7.29 (m, 9H; phenyl H), 6.75 (d, J = 5.6 Hz, 1H; 5′-bpy H), 2.56 (s, 3H; methyl-H), 2.42 ppm (s, 3H; methyl-H); ^{31}P NMR (162 MHz, MeOD): δ = 59.21 ppm; IR (KBr disc): $\tilde{\nu}$ = 2095, 2065 cm^{-1} (C≡N); MS (ESI, negative-ion mode): m/z 626.7 $[M-K]^-$; elemental analyses calcd (%) for **4a**·3H_2O: C 55.14, H 4.63, N, 9.74; found: C 55.28, H 4.48, N 9.88.

***fac*-K[Ru(PPh$_3$)(CN)$_3$(Me$_2$bpy)] (4b)**: Yield: 5.8 % (12 mg, 0.018 mmol); ^{1}H NMR (400 MHz, MeOD): δ = 8.71 (d, J = 5.7 Hz, 2H; 6,6′-bpy H), 8.05 (s, 2H; 3,3′-bpy H), 7.45 (t, J = 8.4 Hz, 6H; phenyl H), 7.22–7.09 (m, 9H; phenyl H), 6.90 (d, J = 4.9 Hz, 2H; 5,5′-bpy H), 2.42 ppm (s, 6H; methyl-H); ^{31}P NMR (162 MHz, MeOD): δ = 41.18 ppm; IR (KBr disc): $\tilde{\nu}$ = 2088, 2063, 2048 cm^{-1} (C≡N); MS (ESI, negative-ion mode): m/z 626.7 $[M-K]^-$; elemental analyses calcd (%) for **4b**·3H_2O: C 55.14, H 4.63, N 9.74; found: C 55.44, H 4.73, N 9.73.

$[Ru(PPh_3)_2(CN)_2(phen)]$ (5): Yield: 14.3 % (38 mg, 0.044 mmol); ^{1}H NMR (400 MHz, $CDCl_3$): δ = 8.83 (d, J = 5.2 Hz, 2H; 2,9-phen H), 7.92 (d, J = 8.0 Hz, 2H; 4,7-phen H), 7.78 (s, 1H; 5,6-phen H), 7.39–7.33 (m, 12H), 7.12 (t, J = 7.3 Hz, 6H; phenyl H), 7.07–7.02 (m, 12H; phenyl H), 6.85 ppm (dd, J = 8.0, 5.2 Hz, 2H; 3,8-phen H); ^{31}P NMR (162 MHz, $CDCl_3$): δ = 38.27 ppm; IR (KBr disc): $\tilde{\nu}$ = 2077, 2062 cm^{-1} (C≡N); MS (ESI, positive-ion mode): m/z 858.7 $[M+H]^+$; elemental analyses calcd (%) for **5**·0.5H_2O: C 69.28, H 4.53, N 6.46; found: C 69.21, H 4.475, N 6.20.

***mer*-K[Ru(PPh$_3$)(CN)$_3$(phen)] (6)**: Yield: 29.8 % (61 mg, 0.092 mmol); ^{1}H NMR (400 MHz, MeOD): δ = 10.17 (m, 1H; 2-phen H), 8.61 (dd, J = 8.2, 1.5 Hz, 1H; 4-phen H), 8.43 (dd, J = 8.3, 1.4 Hz, 1H; 7-phen H), 8.11–8.06 (m, 2H; 5,6-phen H), 8.05 (s, 1H; 9-phen H), 8.03–7.94 (m, 7H; 6 phenyl H and 1 3-phen H), 7.42–7.34 (m, 9H; phenyl H), 7.28 ppm (dd, J = 8.1, 5.2 Hz, 1H; 8-phen H); ^{31}P NMR (162 MHz, MeOD): δ = 58.92 ppm; IR (KBr disc): $\tilde{\nu}$ = 2097, 2066 cm^{-1} (C≡N); MS (ESI, negative-ion mode): m/z 622.1 $[M-K]^-$; elemental analyses calcd (%) for **6**·H_2O: C 58.40, H 3.71, N 10.32; found: C 58.21, H 3.73, N 10.29.

$[Ru\{P(tol)_3\}_2(CN)_2(bpy)]$ (7): Yield: 22.4 % (63 mg, 0.069 mmol); ^{1}H NMR (400 MHz, $CDCl_3$): δ = 8.55 (d, J = 5.6 Hz, 2H; 6,6′-bpy H), 7.67 (d, J = 8.1 Hz, 2H; 3,3′-bpy H), 7.45–7.41 (m, 2H; 4,4′-bpy H), 7.41–7.34 (m, 12H; phenyl H), 6.89 (d, J = 7.7 Hz, 12H; phenyl H), 6.49 (t, J = 6.6 Hz, 2H; 5,5′-bpy H), 2.21 ppm (s, 18H; methyl-H); ^{31}P NMR (162 MHz, $CDCl_3$): δ = 35.82 ppm; IR (KBr disc): $\tilde{\nu}$ = 2074, 2063 cm^{-1} (C≡N); MS (ESI, positive-ion mode): m/z 940.7 $[M+Na]^+$; elemental analyses calcd (%) for **7**·H_2O: C 69.29, H 5.60, N 5.99; found: C 69.32, H 5.21, N 5.77.

***mer*-K[Ru{P(tol)$_3$}(CN)$_3$(bpy)] (8)**: Yield: 32.6 % (68 mg, 0.1 mmol); ^{1}H NMR (400 MHz, MeOD): δ = 9.86 (m, 1H; 6-bpy H), 8.41 (d, J = 7.7 Hz, 1H; 3-bpy H), 8.35 (d, J = 8.4 Hz, 1H; 3′-bpy H), 8.02 (t, J = 8.4 Hz, 1H; 4-bpy H), 7.96 (d, J = 4.4 Hz, 1H; 6′-bpy H), 7.85 (t, J = 7.8 Hz, 1H; 4′-bpy H), 7.80–7.71 (m, 6H; phenyl H), 7.57 (t, J = 7.0 Hz, 1H; 5-bpy H), 7.19–7.11 (m, 6H; phenyl H), 6.91 (t, J = 6.5 Hz, 1H; 5′-bpy H), 2.34 ppm (s, 9H); ^{31}P NMR (162 MHz, MeOD): δ = 55.94 ppm;

IR (KBr disc): $\tilde{\nu}$ = 2099, 2071, 2064 cm^{-1} (C≡N); MS (ESI, negative-ion mode): *m/z* 640.2 $[M-K]^-$; elemental analyses calcd (%) for **8**·3H_2O: C 55.73, H 4.81, N 9.56; found: C 55.83, H 4.47, N 9.36.

[Ru{P(C_6H_4Cl)$_3$}$_2$(CN)$_2$(bpy)] (9): Yield: 12.9% (33 mg, 0.032 mmol); ^{1}H NMR (400 MHz, $CDCl_3$): δ = 8.52 (d, *J* = 5.6 Hz, 2H; 6,6′-bpy H), 7.78 (d, *J* = 8.1 Hz, 2H; 3,3′-bpy H), 7.60 (t, *J* = 7.8 Hz, 2H; 4,4′-bpy H), 7.45–7.39 (m, 12H; phenyl H), 7.15–7.10 (m, 12H; phenyl H), 6.73 ppm (t, *J* = 6.1 Hz, 2H; 5,5′-bpy H); ^{31}P NMR (162 MHz, $CDCl_3$): δ = 36.97 ppm; IR (KBr disc): $\tilde{\nu}$ = 2075, 2062 cm^{-1} (C≡N); MS (ESI, positive-ion mode): *m/z* 1062.4 $[M+Na]^+$; elemental analyses calcd (%) for **9**·0.5H_2O: C 54.93, H 3.17, N 5.34; found: C 54.92, H 3.15, N 4.88.

***mer*-K[Ru{P(C_6H_4Cl)$_3$}(CN)$_3$(bpy)] (10)**: Yield: 31.3% (57 mg, 0.077 mmol); ^{1}H NMR (400 MHz, MeOD): δ = 9.81 (m, 1H; 6-bpy H), 8.45 (d, *J* = 8.2 Hz, 1H; 3-bpy H), 8.40 (d, *J* = 8.1 Hz, 1H; 3′-bpy H), 8.07 (td, *J* = 7.8, 1.6 Hz, 1H; 4-bpy H), 8.03 (d, *J* = 5.6 Hz, 1H; 6′-bpy H), 7.92 (td, *J* = 7.9, 1.5 Hz, 1H; 4′-bpy H), 7.90–7.84 (m, 6H; phenyl H), 7.61 (t, *J* = 6.4 Hz, 1H; 5-bpy H), 7.41–7.36 (m, 6H; phenyl H), 7.05 ppm (ddd, *J* = 7.2, 5.6, 1.3 Hz, 1H; 5′-bpy H); ^{31}P NMR (162 MHz, MeOD): δ = 59.17 ppm; IR (KBr disc): $\tilde{\nu}$ = 2097, 2066 cm^{-1} (C≡N); MS (ESI, negative-ion mode): *m/z* 700.0 $[M-K]^-$; elemental analyses calcd (%) for **10**·0.5Et_2O: C 51.01, H 3.24, N 9.01; found: C 51.38, H 3.62, N 9.19.

[Ru{P(C_6H_4OMe)$_3$}$_2$(CN)$_2$(bpy)] (11): Yield: 18.7% (48 mg, 0.047 mmol); ^{1}H NMR (400 MHz, $CDCl_3$): δ = 8.59 (d, *J* = 5.6 Hz, 2H; 6,6′-bpy H), 7.70 (d, *J* = 8.1 Hz, 2H; 3,3′-bpy H), 7.46 (t, *J* = 8.3 Hz, 2H; 4,4′-bpy H), 7.44–7.38 (m, 12H; phenyl H), 6.65 (d, *J* = 8.4 Hz, 12H; phenyl H), 6.56 (t, *J* = 6.7 Hz, 2H; 5,5′-bpy H), 3.74 ppm (s, 18H; methyl-H); ^{31}P NMR (162 MHz, $CDCl_3$): δ = 34.08 ppm; IR (KBr disc): $\tilde{\nu}$ = 2069, 2055 cm^{-1} (C≡N); MS (ESI, positive-ion mode): *m/z* 1036.7 $[M+Na]^+$; elemental analyses calcd (%) for **11**·H_2O: C 62.84, H 5.08, N 5.43; found: C 62.46, H 4.87, N 5.10.

***mer*-K[Ru{P(C_6H_4OMe)$_3$}(CN)$_3$(bpy)] (12)**: Yield: 31.0% (57 mg, 0.078 mmol); ^{1}H NMR (400 MHz, MeOD): δ = 9.86 (m, 1H; 6-bpy H), 8.41 (d, *J* = 8.2 Hz, 1H; 3-bpy H), 8.35 (d, *J* = 8.1 Hz, 1H; 3′-bpy H), 8.06–7.99 (m, 2H; 4,6′-bpy H), 7.86 (t, *J* = 7.8 Hz, 1H; 4′-bpy H), 7.83–7.74 (m, 6H; phenyl H), 7.57 (t, *J* = 6.5 Hz, 1H; 5-bpy H), 6.96 (t, *J* = 6.5 Hz, 1H; 5′-bpy H), 6.93–6.85 (m, 6H; phenyl H), 3.80 ppm (s, 9H; methyl-H); ^{31}P NMR (162 MHz, MeOD): δ = 53.62 ppm; IR (KBr disc): $\tilde{\nu}$ = 2093, 2064, 2053 cm^{-1} (C≡N); MS (ESI, negative-ion mode): *m/z* 688.2 $[M-K]^-$; elemental analyses calcd (%) for **12**·0.5Et_2O: C 56.61, H 4.49, N 9.17; found: C 56.78, H 4.44, N 9.53.

Acknowledgements

This work was supported by an RGC GRF grant from the Research Grants Council of Hong Kong (Project No. CityU 9041740) and by a grant from the City University of Hong Kong (Project No. 7008183). The photolysis system was supported by a Special Equipment Grant from the University Grants Committee of the Hong Kong SAR, China (SEG CityU02).

[1] a) *The Chemistry of Cyano Complexes of the Transition Metals* (Ed.: A. G. Sharpe), Academic Press, London, **1976**; b) T. P. Hanusa in *Encyclopedia of Inorganic Chemistry, Vol. 2: Cyanide Complexes of the Transition Metals* (Ed.: R. B. King), Wiley, Chichester, **1994**, pp. 943–949.

[2] a) K. Kalyanasundaram, M. Graetzel, M. K. Nazeeruddin, *Inorg. Chem.* **1992**, *31*, 5243–5253; b) M. D. Ward, *Coord. Chem. Rev.* **2006**, *250*, 3128–3141; c) H. Adams, W. Z. Alsindi, G. M. Davies, M. B. Duriska, T. L. Easun, H. E. Fenton, J. Herrera, M. W. George, K. L. Ronayne, X.-Z. Sun, M. Towrie, M. D. Ward, *Dalton Trans.* **2006**, 39–50; d) J. Herrera, M. D. Ward, H. Adams, S. J. A. Pope, S. Faulkner, *Chem. Commun.* **2006**, 1851–1853; e) T. Lazarides, T. L. Easun, C. Veyne-Marti, W. Z. Alsindi, M. W. George, N. Deppermann, C. A. Hunter, H. Adams, M. D. Ward, *J. Am. Chem. Soc.* **2007**, *129*, 4014–4027; f) M. D. Ward, *Dalton Trans.* **2010**, *39*, 8851–8867; g) R. Argazzi, C. A. Bignozzi, M. Yang, G. M. Hasselmann, G. J. Meyer, *Nano Lett.* **2002**, *2*, 625–628.

[3] a) C. A. Bignozzi, C. Chiorboli, M. T. Indelli, M. A. Rampi Scandola, G. Varani, F. Scandola, *J. Am. Chem. Soc.* **1986**, *108*, 7872–7873; b) C. J. Timpson, C. A. Bignozzi, B. P. Sullivan, E. M. Kober, T. J. Meyer, *J. Phys. Chem.* **1996**, *100*, 2915–2925; c) T. Abe, T. Suzuki, K. Shinozaki, *Inorg. Chem.* **2010**, *49*, 1794–1800; d) S. Encinas, A. F. Morales, F. Barigelletti, A. M. Barthram, C. M. White, S. M. Couchman, J. C. Jeffery, M. D. Ward, D. C. Grills, M. W. George, *J. Chem. Soc. Dalton Trans.* **2001**, 3312–3319; e) T. L. Easun, W. Z. Alsindi, N. Deppermann, M. Towrie, K. L. Ronayne, X.-Z. Sun, M. D. Ward, M. W. George, *Inorg. Chem.* **2009**, *48*, 8759–8770; f) M. Kovács, A. Horváth, *J. Photochem. Photobiol. A* **2004**, *163*, 13–19; g) M. E. García Posse, N. E. Katz, L. M. Baraldo, D. D. Polonuer, C. G. Colombano, J. A. Olabe, *Inorg. Chem.* **1995**, *34*, 1830–1835; h) S. G. Baca, H. Adams, C. S. Grange, A. P. Smith, I. Sazanovich, M. D. Ward, *Inorg. Chem.* **2007**, *46*, 9779–9789; i) L. T.-L. Lo, S.-W. Lai, S.-M. Yiu, C.-C. Ko, *Chem. Commun.* **2013**, *49*, 2311–2313.

[4] a) J. K. Evju, K. R. Mann, *Chem. Mater.* **1999**, *11*, 1425–1433; b) N. R. M. Simpson, M. D. Ward, A. F. Morales, B. Ventura, F. Barigelletti, *J. Chem. Soc. Dalton Trans.* **2002**, 2455–2461; c) M. T. Indelli, M. Ghirotti, A. Prodi, C. Chiorboli, F. Scandola, N. D. McClenaghan, F. Puntoriero, S. Campagna, *Inorg. Chem.* **2003**, *42*, 5489–5497.

[5] a) L. A. Sacksteder, A. P. Zipp, E. A. Brown, J. Streich, J. N. Denas, B. A. DeGraff, *Inorg. Chem.* **1990**, *29*, 4335–4340; b) J. V. Caspar, T. J. Meyer, *J. Phys. Chem.* **1983**, *87*, 952–957; c) C.-C. Ko, A. W.-Y. Cheung, L. T.-L. Lo, J. W.-K. Siu, C.-O. Ng, S.-M. Yiu, *Coord. Chem. Rev.* **2012**, *256*, 1546–1555.

[6] For the characterization data of $K_2[Ru(CN)_4(PR_3)_2]$, see the Supporting Information.

[7] a) *^{31}P and ^{13}C NMR of Transition Metal Phosphine Complexes* (Eds.: P. S. Pregosin, R. W. Kunz), Springer, Heidelberg, **1979**, pp. 65–68; b) W. H. Hersh, P. Xu, B. Wang, J. W. Yom, C. K. Simpson, *Inorg. Chem.* **1996**, *35*, 5453–5459; c) M. D. Fryzuk, C. D. Montgomery, S. J. Rettig, *Organometallics* **1991**, *10*, 467–473; d) Y.-J. Kim, S.-C. Lee, M. H. Cho, S.-W. Lee, *J. Organomet. Chem.* **1999**, *588*, 268–277.

[8] a) P. Chen, M. Curry, T. J. Meyer, *Inorg. Chem.* **1989**, *28*, 2271–2280; b) L. T.-L. Lo, C.-O. Ng, H. Feng, C.-C. Ko, *Organometallics* **2009**, *28*, 3597–3600; c) C.-C. Ko, L. T.-L. Lo, C.-O. Ng, S.-M. Yiu, *Chem. Eur. J.* **2010**, *16*, 13773–13782; d) A. W.-Y. Cheung, L. T.-L. Lo, C.-C. Ko, S.-M. Yiu, *Inorg. Chem.* **2011**, *50*, 4798–4810; e) C.-O. Ng, S.-W. Lai, H. Feng, S.-M. Yiu, C.-C. Ko, *Dalton Trans.* **2011**, *40*, 10020–10028.

[9] *CRC Handbook of Chemistry and Physics* (Ed.: D. R. Lide), CRC Press, Boca Raton, **2005**, Section 9, pp. 44.

[10] a) D. B. Dell'Amico, F. Calderazzo, U. Englert, L. Labella, F. Marchetti, M. Specos, *Eur. J. Inorg. Chem.* **2004**, 3938–3945; b) J. Xiang, L. T.-L. Lo, C.-F. Leung, S.-M. Yiu, C.-C. Ko, T.-C. Lau, *Organometallics* **2012**, *31*, 7101–7108.

[11] a) C. Reichardt, *Angew. Chem.* **1965**, *77*, 30–40; *Angew. Chem. Int. Ed. Engl.* **1965**, *4*, 29–40; b) C. Reichardt, *Chem. Rev.* **1994**, *94*, 2319–2358; c) C.-O. Ng, L. T.-L. Lo, S.-M. Ng, C.-C. Ko, N. Zhu, *Inorg. Chem.* **2008**, *47*, 7447–7449; d) C.-C. Ko, J. W.-K. Siu, A. W.-Y. Cheung, S.-M. Yiu, *Organometallics* **2011**, *30*, 2701–2711.

[12] a) P. Hummel, J. Oxgaard, W. A. Goddard III, H. B. Gray, *J. Coord. Chem.* **2005**, *58*, 41–45; b) K. J. Nelson, I. D. Giles, W. W. Shum, A. M. Arif, J. S. Miller, *Angew. Chem.* **2005**, *117*, 3189–3192; *Angew. Chem. Int. Ed.* **2005**, *44*, 3129–3132; c) M. Nakamura, *Angew. Chem.* **2009**, *121*, 2676–2678; *Angew. Chem. Int. Ed.* **2009**, *48*, 2638–2640; d) J. Cirera, S. Alvarez, *Dalton Trans.* **2013**, *42*, 7002–7008.

[13] a) D. J. Stufkens, *Comments Inorg. Chem.* **1992**, *13*, 359–385; b) T. G. Kotch, A. J. Lees, *Inorg. Chem.* **1993**, *32*, 2570–2575.

[14] M. A. Rampi, M. T. Indelli, F. Scandola, F. Pina, A. J. Parola, *Inorg. Chem.* **1996**, *35*, 3355–3361.

[15] P. S. Hallman, T. A. Stephenson, G. Wilkinson, *Inorg. Synth.* **1970**, *12*, 237–239.

[16] R. A. Krause, C. Violette, *Inorg. Chim. Acta* **1986**, *113*, 161–162.
[17] J. N. Demas, G. A. Crosby, *J. Phys. Chem.* **1971**, *75*, 991.
[18] a) K. Suzuki, A. Kobayashi, S. Kaneko, K. Takehira, T. Yoshihara, H. Ishida, Y. Shiina, S. Oishi, S. Tobita, *Phys. Chem. Chem. Phys.* **2009**, *11*, 9850–9860; b) H. Ishida, S. Tobita, Y. Hasegawa, R. Katoh, K. Nozaki, *Coord. Chem. Rev.* **2010**, *254*, 2449–2458.
[19] a) G. M. Sheldrick, SHELXS-97 and SHELXL-97, Programs for Crystal Structure Solution and Refinement, University of Göttingen, Germany, **1997**; b) G. M. Sheldrick, *Acta Crystallogr. Sect. A* **2008**, *64*, 112–122.

Received: June 11, 2013
Published online: ■■ ▮▮, 0000

Luminescent Complexes

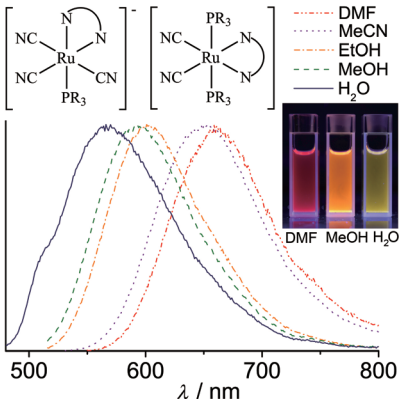

Strongly emissive cyanoruthenates: New classes of highly solvatochromic luminescent cyanoruthenium(II) and cyanoruthenate(II) complexes with significantly improved emission quantum efficiencies and lifetimes compared with the well-studied tetracyanoruthenate systems have been developed. Their photophysical properties, solvatochromism, and electrochemistry have also been investigated (see figure).